Accelerated Publications

Out-of-Shape DNA Minor Groove Binders: Induced Fit Interactions of Heterocyclic Dications with the DNA Minor Groove†

Yi Miao,‡ Michael P. H. Lee,§ Gary N. Parkinson,§ Adalgisa Batista-Parra,‡ Mohamed A. Ismail,‡ Stephen Neidle,*,§ David W. Boykin,*,‡ and W. David Wilson*,‡

Department of Chemistry, Georgia State University, Atlanta, Georgia 30303, and Cancer Research UK Biomolecular Structure Group, The School of Pharmacy, University of London, London WC1N 1AX, U.K.

Received September 6, 2005; Revised Manuscript Received September 30, 2005

ABSTRACT: DB921 and DB911 are benzimidazole-biphenyl isomers with terminal charged amidines. DB911 has a central meta-substituted phenyl that gives it a shape similar to those of known minor groove binding compounds. DB921 has a central para-substituted phenyl with a linear conformation that lacks the appropriate radius of curvature to match the groove shape. It is thus expected that DB911, but not DB921, should be an effective minor groove binder, but we find that DB921 not only binds in the groove but also has an unusually high binding constant in SPR experiments (2.9×10^8 M^{-1}, vs 2.1×10^7 M^{-1} for DB911). ITC thermodynamic analysis with an AATT sequence shows that the stronger binding of DB921 is due to a more favorable binding enthalpy relative to that of DB911. CD results support minor groove binding for both compounds but do not provide an explanation for the binding of DB921. X-ray crystallographic analysis of DB921 bound to AATT shows that an induced fit structural change in DB921 reduces the twist of the biphenyl to complement the groove, and places the functional groups in position to interact with bases at the floor of the groove. The phenylamidine of DB921 forms indirect contacts with the bases through a bound water. The DB921−water pair forms a curved binding module that matches the shape of the minor groove and provides a number of strong interactions that are not possible with DB911. This result suggests that traditional views of compound curvature required for minor groove complex formation should be reevaluated.

Eukaryotic parasitic diseases, such as sleeping sickness, are caused by ancient, unusual, and quite deadly microorganisms (*1*). The sleeping sickness parasite, *Trypanosoma brucei*, limits the health and economic hopes of millions of people, and if not effectively treated, the disease is fatal (*2*). Unfortunately, many of the drugs used to treat the disease are quite toxic and are related to compounds from as far back as the pioneering work of Ehrlich on parasitic disease (*3*). Dicationic diamidines such as furamidine (DB75, Figure 1), berenil, and pentamidine have exhibited significant activity against parasitic diseases and are a promising class for the development of new drugs (*4*). Dications enter parasite cells slowly by diffusion, but there are transporters that can effectively carry them into cells (*5*). Fluorescence microscopy with the intrinsic fluorescence of the diamidines indicates that after the compounds are transported, they move rapidly and in high concentration to the mitochondrial kinetoplast that is present in trypanosomes and *Leishmania* parasites (*6*). The kinetoplasts subsequently disappear, and then the parasites die.

The thousands of DNA minicircles with A·T rich sequence tracts in the kinetoplast provide a large array of binding sites for A·T specific compounds (*7*, *8*). In the first stages of drug action, on the basis of fluorescence analysis, kinetoplast DNA (kDNA) binding accounts for much of the compound in the parasite cells, and the cytoplasm contains quite low concentrations of the drug (*6*). These results strongly suggest that A·T rich regions of the kDNA minicircles are the critical target of diamidines. The disappearance of the kinetoplast after compound uptake suggests that the diamidines interfere with the complex replication of the catenated kDNA. Our strategy to capitalize on these observations and intrinsic features of the heterocyclics involves design and development of new compounds targeted to A·T sequences in the DNA minor groove in a variety of complexes that have limited toxicity and good cell uptake properties in parasites.

Classical minor groove binding compounds are unfused heterocyclic cations such as DB75 (*9*, *10*), and it has been proposed that there are strict limits on their structures for

† Research at Georgia State University was supported by National Institutes of Health Grants GM61587 and AI 46365. BIAcore and ITC instruments were funded in part by the Georgia Research Alliance. Research at the University of London was supported by a program grant from Cancer Research UK.

* To whom correspondence should be addressed. W.D.W.: telephone, (404) 651-3903; fax, (404) 651-2751; e-mail, wdw@gsu.edu. S.N.: e-mail, stephen.neidle@ulsop.ac.uk. D.W.B.: e-mail, dboykin@gsu.edu.

‡ Georgia State University.

§ University of London.

10.1021/bi051791q CCC: $30.25
Published on Web 10/21/2005

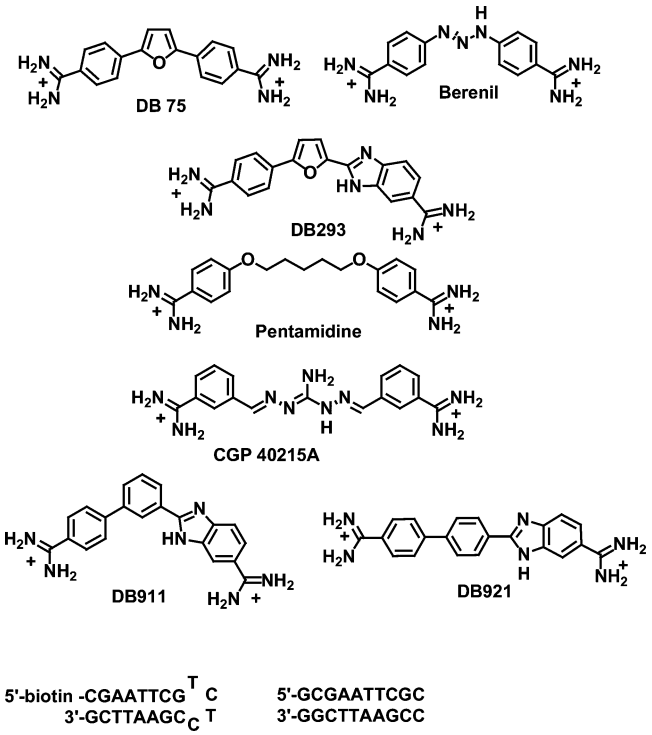

FIGURE 1: Compound structures and DNA hairpin and self-complementary duplex sequences.

DNA complex formation (*11*, *12*). Rules for compound design, for example, have been derived on the basis of a stringent set of compound curvature and functional group positioning criteria that are based on experiments (*12*). Two recent observations, however, have led us to question whether such design limitations are required. First, DB293 (Figure 1) was found to form an unusual stacked tetracationic dimer that can recognize mixed DNA sequences in a complex that does not fit the usual rules (*13*, *14*). Second, the linear diamidine CGP40215 (Figure 1) was found to bind quite strongly to AT sequences, although it does not match the curvature of the minor groove (*15*, *16*). Structural analysis of CGP in an AATT binding site provided an explanation for the binding and showed that a bound water forms a direct contact between an amidine group of the compound and A·T base pair groups at the floor of the groove. The water molecule essentially rescues the linear molecule for DNA binding and completes its curvature for strong minor groove interactions. The CGP−water interaction results in a ternary complex with DNA that matches the shape of the minor groove. Direct H-bonds from one amidine group and an NH group in the nitrogen rich linker are formed to A·T base pairs in the binding site. The amidine at the other end of the molecule is away from the floor of the groove due to the lack of curvature of CGP40215, but it forms indirect H-bonds with DNA through the bound water.

Since compounds with nonstandard binding modes might exhibit new types of antiparasitic action, the results described above stimulated our interest in the design of nonclassical minor groove binding agents that do not perfectly match the shape of the minor groove, especially benzimidazole derivatives related to DB293 and compounds such as CGP. Understanding the limits of minor groove complex formation by compounds that do not fit the classical model should also extend our understanding of DNA molecular recognition. With the sequencing of the human genome, directly targeting genes that are linked to disease for regulation of protein levels is a promising drug development rationale that is independent of parasite therapeutics. New types of compounds that target DNA in different ways can thus have many fundamental and applied uses.

We report here the interaction with DNA of two isomeric biphenyl-benzimidazole diamidine derivatives by using biosensor-surface plasmon resonance, circular dichroism, isothermal titration microcalorimetry, and X-ray crystallography/molecular modeling methods. DB911 (Figure 1) has a central meta-substituted phenyl that gives it a classical type curvature similar to that of DB75 and related minor groove binding agents. DB921 has a central para-substituted phenyl that gives it a much more linear shape that clearly cannot match the curvature of the DNA minor groove. The biphenyl component of both compounds is expected to be significantly twisted. Surprisingly, we find that the linear compound DB921 binds to A·T sequences in DNA much more strongly than either DB75 or the isomer, DB911. X-ray crystallographic analysis of DB921 bound to an AATT sequence has provided an explanation for the binding and suggests that, as with CGP40215 (Figure 1), a water molecule is able to complete the curvature of DB921 for minor groove interactions.

MATERIALS AND METHODS

Compounds, DNAs, and Buffers. DB921 and DB911 were synthesized as previously described (*17*, *18*). Poly(dA)·poly(dT) from Pharmacia Co. was used for T_m[1] experiments. 5′-Biotin-labeled hairpin DNA oligomers were from Midland Certified Reagent Co. MES buffers contained 0.01 M MES and 0.001 M EDTA adjusted to pH 6.25. MES00, MES10, and MES20 buffers contained the components given above and 0, 0.1, and 0.2 M NaCl, respectively.

Thermal Melting (T_m). T_m experiments were conducted with a Cary 300 UV−visible spectrophotometer in 1 cm quartz cuvettes. The absorbance of the DNA−compound complex was monitored at 260 nm as a function of temperature, and DNA without compound was used as a control. Cuvettes were mounted in a thermal block, and the solution temperatures were monitored with a thermistor in a reference cuvette with a computer-controlled heating rate of 0.5 °C/min. A ratio of 0.3 compound per DNA base was used for the complex with poly(dA)·poly(dT).

Circular Dichroism (CD). CD spectra were collected with a Jasco J-710 spectrometer at different ratios of compound to DNA at 25 °C in MES10 buffer. The DNA was added to buffer in a 1 cm quartz cuvette and scanned over a desired wavelength range. The compounds at increasing ratios were then titrated into DNA, and the complexes were rescanned under the same conditions.

Biosensor-Surface Plasmon Resonance (SPR). Biosensor-SPR experiments were conducted with a BIAcore 3000 (Biacore, Uppsala, Sweden) instrument as previously described (*13*−*16*). 5′-Biotin-labeled DNA hairpins were immobilized on four-channel BIAcore SA sensor chips via

[1] Abbreviations: SPR, surface plasmon resonance; ITC, isothermal titration calorimetry; CD, circular dichroism; MES, 2-(*N*-morpholino)-ethanesulfonic acid; T_m, thermal melting temperature of DNA where the duplex is 50% unfolded.

noncovalent streptavidin capture. Three flow cells contained DNA, and one flow cell was left blank as a reference. The compounds at different diluted concentrations in the degassed and filtered MES20 buffer with 0.005% surfactant P-20 were injected over the DNA surface for selected times. A glycine solution (10 mM, pH 2.0) was used for regeneration. Steady-state binding studies were carried out by averaging the resonance unit values (RU) over a selected time region at different compound concentrations and converting them to r (moles of bound compound per mole of DNA hairpin); $r = RU_{eq}/RU_{max}$, where RU_{eq} is the averaged RU at steady state for each concentration and RU_{max} is the maximum RU value for binding one compound per binding site. The binding constant, K_a, was obtained from the best fit of r versus free compound concentration (C_{free}) with a one-site binding model

$$r = (K_a C_{free})/(1 + K_a C_{free}) \quad (1)$$

Fits with more than one site did not improve the correlation coefficient or residuals significantly for either DB921 or DB911. Kinetic analysis was performed by global fitting of the binding data with non-mass-transport and mass-transport-limited kinetic 1:1 binding models (*19*, *20*). In the non-mass-transport 1:1 binding model, eq 2 is used, while in the mass-transport-limited model, eqs 2 and eq 3 are used.

$$A + B \leftrightarrow AB \quad K_a = [AB]/[A][B] = k_a/k_d$$

$$[A]_{t=0} = 0,\ [B]_{t=0} = RU_{max},\ [AB]_{t=0} = 0$$

$$d[AB]/dt = k_a[A][B] - k_d[AB] \quad (2)$$

$$d[A]/dt = k_t([A_{bulk}] - [A]) - (k_a[A][B] - k_d[AB]) \quad (3)$$

where [A] and $[A_{bulk}]$ are the concentrations of the compound at the sensor surface and the in the bulk solution, respectively, [B] is the concentration of the immobilized DNA without bound compound, and [AB] is the concentration of the complex; k_a is the association and k_d the dissociation rate constant.

Isothermal Titration Calorimetry (ITC). ITC experiments were performed with a MicroCal VP-ITC instrument (MicroCal Inc., Northampton, MA) interfaced with a computer equipped with VP-2000 viewer instrument control software. ITC data were analyzed with Origin 5.0. In ITC experiments, 10 μL of compound in MES20 buffer was injected into the instrument sample cell containing the AATT DNA duplex in MES20 buffer for each injection. The observed heat for each injection was measured by integration of the area of power peak with respect to time. Blank titrations were conducted by injecting the compound into the sample cell containing only buffer under the same conditions. The corrected interaction heat was determined by subtracting the blank heat from that for the compound/DNA titration.

Crystallography. DB921 was cocrystallized by the hanging-drop method with the sequence $d(CGCGAATTCGCG)_2$ from a drop containing 9.375 mM $MgCl_2$, 0.375 mM duplex DNA, 0.5 mM DB921, 3.125% (v/v) (±)-2-methyl-2,4-pentanediol (MPD), and 20 mM sodium cacodylate buffer at pH 6.5, equilibrated against a reservoir of a 50% (v/v) MPD solution. The crystals, in space group $P2_12_12_1$, were isomorphous with other minor groove drug structures, and their structures were determined by molecular replacement using 7968 unique reflections to a resolution of 1.64 Å (96% completeness) collected with an in-house image plate system on a flash-frozen crystal. The final R factor and R_{free} values were 21.4 and 28.5%, respectively, with the inclusion of 76 water molecules and a hydrated magnesium ion. Full details are available as Supporting Information; atomic coordinates and structure factors have been deposited in the Protein Data Bank as entry 2B0K and in the Nucleic Acid Database as entry DD0074.

RESULTS AND DISCUSSION

Thermal Melting. Thermal melting enables the rapid qualitative evaluation of the relative binding affinities of compounds for DNA (*21*). As part of a screen to find new antiparasitic agents that target AT sequences of parasite kDNA, ΔT_m values for DB921 and DB911 with poly(dA)·poly(dT) were compared to that for the well-characterized reference compound DB75 (ΔT_m = 24.8 °C in MES10 buffer), under the same conditions. Converting the furan of DB75 to a similarly shaped meta-substituted phenyl group (DB911, ΔT_m = 25.3 °C) does not significantly change the stability of the complex. Surprisingly, however, changing the central group from a meta- to para-substituted phenyl (DB921) results in a significant increase in melting temperature. The binding of DB921 is so strong that the complex with poly(dA)·poly(dT) DNA unfolds above 95 °C, and no melting transition was observed (ΔT_m > 28 °C). Thermal melting results with an AATT DNA hairpin duplex with a lower T_m were studied at compound:oligomer duplex ratios of 1:1, 2:1, and 3:1. The results suggest that DB921 binds to the AATT DNA sequence with 1:1 stoichiometry since the T_m is not significantly increased at ratios above 1:1. The ΔT_m values for DB911 and DB921 are 19.8 and 25.9 °C, respectively, with the AATT hairpin duplex. ΔT_m values for both compounds were quite low for DNA sequences that contain only G·C base pairs (not shown). These results clearly indicate DB921 has a binding affinity for A·T DNA sequences that is much greater than that expected on the basis of its molecular structure.

Circular Dichroism. Given the strong binding of DB921 to A·T DNA, a critical question is whether it has a similar mode of binding to DB75 and DB911. To probe the mode of binding, CD spectra of DB921 and DB911 with the AATT DNA hairpin used in T_m studies were monitored. At the maximum absorption wavelengths of the compounds, 325 nm (DB921) and 315 nm (DB911), where the DNA CD signals do not interfere, positive induced CD signals were observed (Supporting Information, Figure S1). Positive induced CD signals are generally a characteristic of binding in the minor groove of DNA (*22*, *23*). Interestingly, the induced positive CD signal of DB921 is not as large as that of DB911 or that generally expected for strong binding in the minor groove of AT sequences. Small induced CD changes on binding to DNA may be a characteristic of linear compounds (*16*). No significant CD signals were observed upon addition of DB921 or DB911 to GC sequence DNA under the same conditions. At much higher concentrations, small induced CD signals were observed for DB911 with GC sequences, perhaps due to partial intercalation as observed for DB75 with GC sequences (*22*). In summary,

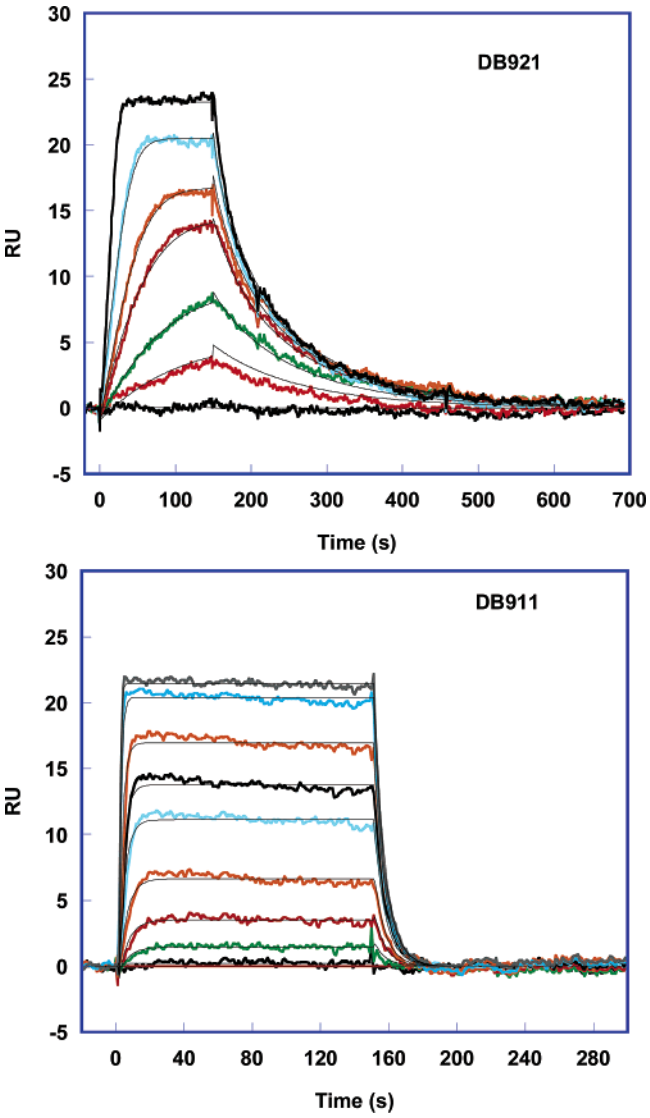

FIGURE 2: SPR sensorgrams for binding of DB921 (top) and DB911 (bottom) with the immobilized AATT DNA hairpin in MES20 buffer. The black lines are best fit curves determined by global kinetic fitting. For DB921, the concentrations from bottom to top are 0, 0.001, 0.0015, 0.002, 0.003, 0.004, 0.006, 0.008, and 0.01 μM. For DB911, the concentrations from bottom to top are 0, 0.004, 0.01, 0.02, 0.04, 0.06, 0.1, 0.2, and 0.4 μM.

CD results indicate that both DB921 and DB911 bind in the DNA minor groove in AT sequences.

Biosensor-Surface Plasmon Resonance (SPR). Biosensor-SPR methods provide an excellent way of quantitatively comparing the interactions between small molecules and DNA (*24*−*26*). Because of the strong binding and relatively weak spectroscopic signals of the diamidines at typical experimental concentrations (typically sub-nanomolar to 1 μM), it is difficult to determine their *K* values by spectroscopy. Calorimetric and other potential methods have similar limitations where strong binding is obtained. Because SPR with immobilized DNA responds to the mass of the bound species, it can be used for diamidines that have large variations in properties, such as *K* values.

SPR sensorgrams for the binding of DB921 and DB911 with a DNA hairpin duplex that contains a single AATT binding site (Figure 1) are compared in Figure 2. Similar experiments with an oligomer hairpin with only G·C base pairs did not exhibit any detectable binding (not shown). For steady-state analysis, K_a was determined from the nonlinear least-squares best fit to a single-binding site model (Materials and Methods). For kinetic data analysis, association (k_a) and dissociation rate constants (k_d) were determined by global fitting of the binding data (Figure 2). The kinetic K_a was derived from the ratio of association and dissociation rate constants (Table 1). The interaction kinetics of DB921 with DNA under the experimental conditions are dominated by mass transport from the bulk solution to the biosensor interaction matrix. As expected for mass-transport-limited rates, the kinetic data are quite different when fitting with mass-transport versus non-mass-transport kinetic models, and when changing the flow rate (*20*). The calculated k_aRU_{max}/k_t ratios are greater than 5, providing further evidence for mass-transport-limited binding rates since the ratio of less than 5 has been shown to be important for obtaining reliable kinetic data (*20*). Reliable binding affinities, however, can be obtained from SPR results under these conditions, and the binding affinity for DB921 derived from the kinetic model is in good agreement with K_a values from steady-state results (Table 1). The binding of DB911 to the AATT hairpin is weaker than for DB921 and, under the experimental conditions of Figure 2, is not mass-transport-limited. For DB911, the association and dissociation rate constants as well as the K_a value (Table 1) obtained from global fits with mass-transport kinetic models are consistent with non-mass-transport-limited binding kinetics. In summary, SPR results quantitatively demonstrate that DB921 with a nonclassical, linear shape binds very strongly to AATT DNA. Its binding affinity is more than 10 times greater than that for DB911 and DB75. Both DB921 and DB911 have a single strong binding site on the AATT DNA hairpin.

Isothermal Titration Calorimetry (ITC). ITC experiments with an AATT sequence oligomer were conducted in an effort to obtain a full thermodynamic understanding of the DB921 and DB911 interactions as well as the basis for the exceptionally strong binding of DB921 (*27*). Titration of DB921 into buffer and into a DNA solution provided plots of heat versus molar ratio (Figure 3). Because of the strong binding of DB921 and DB911 and the relatively small heats of interaction, only ΔH and not *K* could be obtained from the ITC experiments. Because of the lower binding enthalpy for DB911, we have also performed experiments at higher concentrations of DB911 and DNA to improve the results so that the signal-to-noise ratio was like that with DB921

Table 1: Kinetics and Thermodynamics Results in MES20 at 25 °C

	k_a (M^{-1} s^{-1})	k_d (s^{-1})	K_a (k_a/k_d) (M^{-1})	K_a (steady state) (M^{-1})	ΔH (kcal/mol)	$-T\Delta S^a$ (kcal/mol)
DB921	−	−	2.9×10^8	2.7×10^8	−4.5	−7.0
DB911	3.26×10^6	0.153	2.1×10^7	1.9×10^7	−2.5	−7.5

[a] Calculated using the average $\Delta G°$ value from the kinetics and steady state.

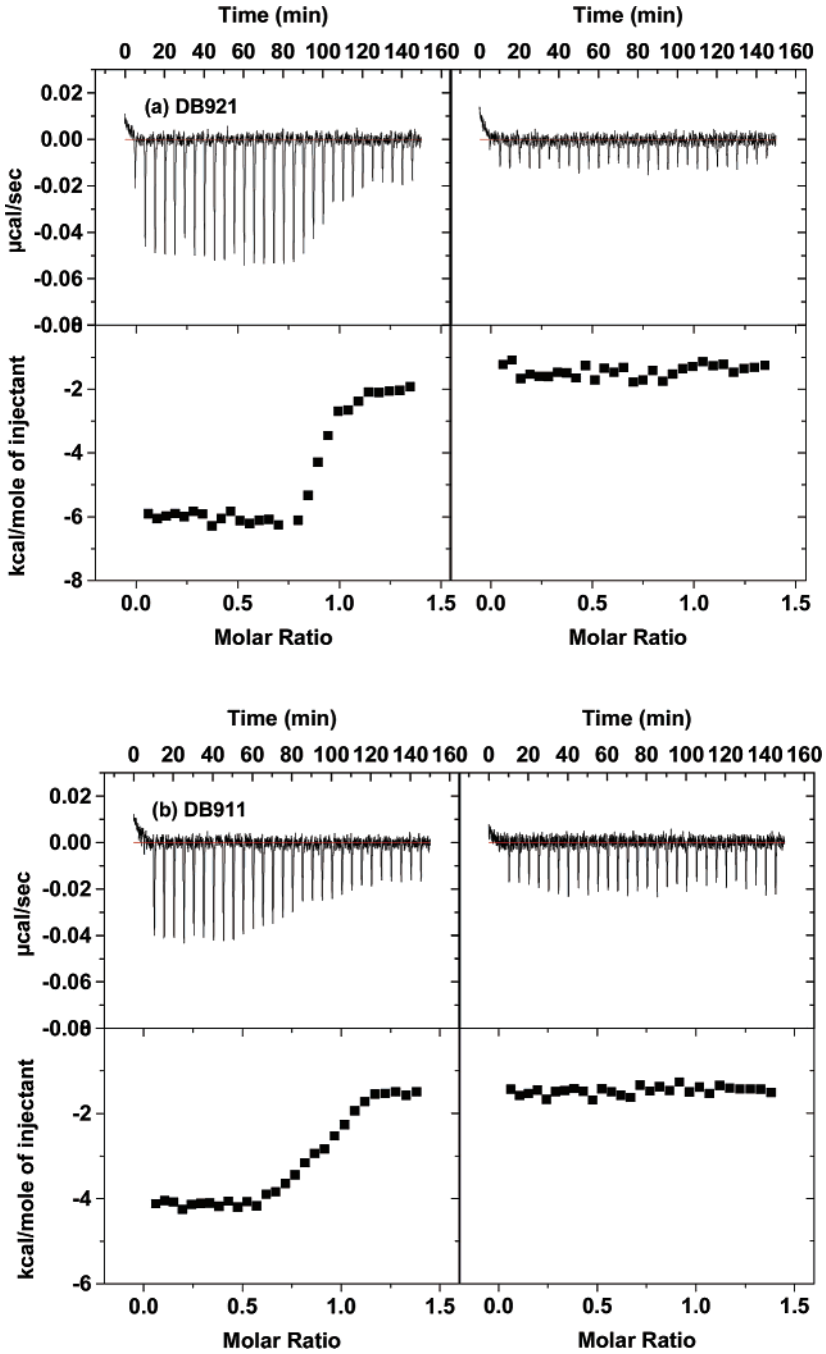

FIGURE 3: ITC experimental curves at 25 °C for (a) titration of 0.025 mM DB921 into 0.004 mM d(GCGAATTCGC)$_2$ duplex (left) and MES20 buffer (right). (b) Titration of 0.025 mM DB911 into 0.004 mM d(GCGAATTCGC)$_2$ duplex (left) and MES20 buffer (right). The average heat per mole of compound at molar ratios of 0.1−0.6 was used to calculate ΔH.

(Supporting Information, Figure S2). The observed binding ΔH for DB921 at 25 °C is -4.5 ± 0.1 kcal/mol; the ΔH value for DB911 is significantly lower, -2.5 ± 0.1 kcal/mol. The calculated $-T\Delta S$ values based on the SPR binding free energies ($\Delta G° = -RT \ln K = -11.5$ kcal/mol for DB921 and −10.0 kcal/mol for DB911) and ΔH values from ITC are −7.0 kcal/mol for DB921 and −7.5 kcal/mol for DB911. These results clearly show that the stronger binding of DB921 is entirely due to a more favorable binding enthalpy.

Although the thermodynamic differences between DB921 and DB911 are undoubtedly due to a number of factors, the strong similarity of the structural isomers significantly limits some of the factors. The similarity of the structure of DB911 to compounds such as DB75, berenil, and pentamidine (Figure 1) suggests that it will form a complex with both amidines H-bonded to DNA bases as with the compounds listed above. DB921, however, requires a connecting water molecule to interact indirectly with the base pairs at one end of the complex (Figure 4). It is interesting that the favorable $\Delta(\Delta H)$ and unfavorable $\Delta(\Delta S)$ values for the differences between binding thermodynamics of DB921 and DB911 are in the range predicted by Dunitz (*28*) and Cooper and coworkers (*29, 30*) for a bound water in compound−biopolymer complexes. The $\Delta(\Delta H)$ value is toward the higher end of the estimates, while the $\Delta(\Delta S)$ is at the lower end, indicating, as expected, that other factors are involved. Certainly at the qualitative level, however, the observed

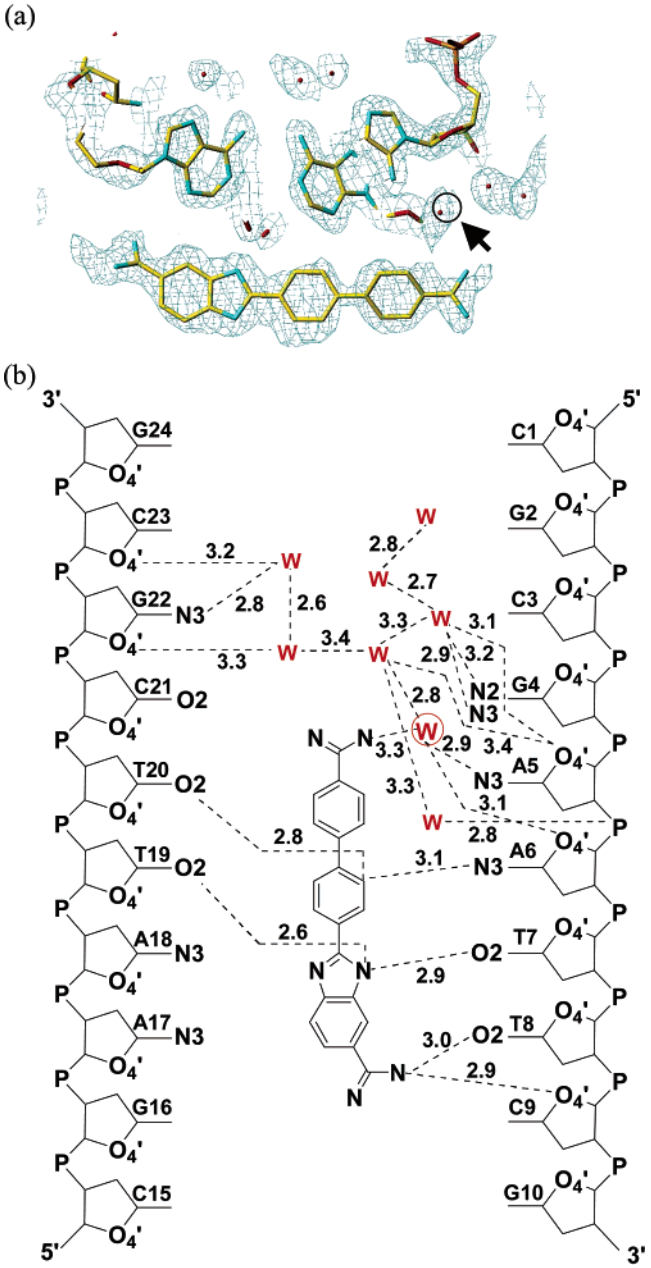

FIGURE 4: (a) Electron density map calculated with the final refined coordinates and drawn in the plane of the DB921 molecule, showing the asymmetric fit of the drug in the groove. The drug is seen to be farther from the edges of the base pairs in the groove on the right-hand side of the figure. Contours have been drawn at the 1.0σ level. (b) Schematic showing the hydrogen bonding distances involving the DB921 molecule, the d(CGCGAATTCGCG)$_2$ structure, and associated water molecules. Twenty of 24 bases are shown. The circled water molecule in panels a and b is the key bound water which forms H-bonds with both DB921 and DNA.

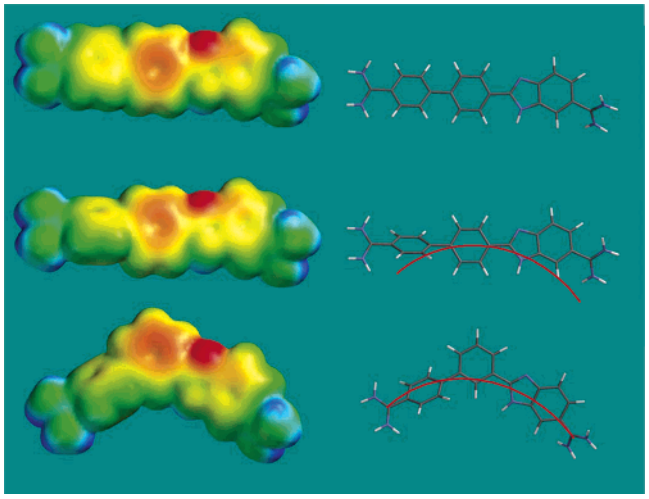

FIGURE 5: Equilibrium geometry of DB911 calculated by the Hartree−Fock approximation at the 321G* level (bottom) and equilibrium geometry of DB921 calculated in the same way (middle). The top structure is DB921 as in the crystal complex. Tube models are shown at the right with space filling electrostatic potential molecular surfaces at the left. The crystal structure of DB921 was frozen in the calculations for comparison to the unconstrained low-energy conformations of DB921 and DB911. A red arc is drawn on the DB911 tube structure (bottom) from amidine carbon to amidine carbon. The same arc is shown superimposed on the DB921 calculated structure (center).

thermodynamics values support the experimental and theoretical analyses of Dunitz (*28*) and Cooper (*29*) for the influence of a bound water.

X-ray Crystallography. The crystal structure of the DB921−d(CGCGAATTCGCG)$_2$ complex has one DB921 molecule binding in the minor groove within the central 5′-AATT region, with one amidinium group (benzimidazole side) anchored in the groove and the other (phenyl side) off the groove floor (Figure 4). The structure shows that the radius of curvature of DB921 is much greater than the corresponding radius of the DNA minor groove. The two phenyl rings of DB921 are twisted with a dihedral angle of 28°. The amidinium groups are also twisted out of plane, by 32° and 43° for the phenyl and benzimidazole amidine linkages, respectively. The binding affinity and specificity involve both direct H-bonds and water-mediated H-bonds. The amidinium group at the benzimidazole end is hydrogen-bonded to O2 of thymine 8 (3.0 Å), and is near O4′ of cytosine 9 on the same strand (2.9 Å). The inner-facing nitrogen atom of the benzimidazole ring forms a pair of bifurcated hydrogen bonds with the O2 atoms of thymine 7 (2.9 Å) and thymine 19 (2.6 Å). The amidinium group at the other end of the molecule does not directly contact the DNA. Instead, it forms a hydrogen bond (3.3 Å) to a water molecule that is part of a network in the minor groove in this region (Figure 4), and which hydrogen bonds to N3 of adenine 5 (2.9 Å). This water molecule is performing a key bridging role, hydrogen bonding to the base pairs at the end of the binding site as well as to DB921. There are also two short C−H···N/O stabilizing interactions from the inner-facing edge of the central phenyl ring to N3 of adenine 6 (3.1 Å) and to O2 of thymine 20 (2.8 Å). Thus, DB921 covers 4 of 5 bp of the binding site with strong interactions by virtue of four strong hydrogen bonds that arise from just the amidine−benzimidazole group and water-mediated hydrogen bonds.

Molecular Structural Comparisons and Models. Geometry-optimized models for DB921 and DB911 were compared to DB921 from the crystal structure (Figure 5). Without the constraints of DNA minor groove binding, both molecules have a significant twist at the phenyl−phenyl bond of ca. 50°. In the crystal structure, this is reduced to <28°. In the calculated structures of both DB921 and DB911, the amidine to aromatic ring dihedral angles are 40 ± 1°. The benzimidazole−amidine angle in the crystal structure is similar, 43°, while the phenyl−amidine angle is reduced to 32°. The benzimidazole−phenyl angle in both the calculated and

crystal structures of DB921 is 0−1°. These results indicate that the amidine−benzimidazole−phenyl end of DB921 undergoes only small structural changes upon formation of the AATT minor groove complex, while the amidine−phenyl−phenyl end undergoes considerable flattening.

The dramatic difference in molecular curvature between isomers DB911 and DB921, which is described above, can also be seen from the comparisons in Figure 5. To illustrate the difference, an arc from amidine carbon to amidine carbon has been overlaid on DB911 (Figure 5). The same arc on DB921 illustrates the lack of appropriate curvature and the requirement that such compounds have for a water interaction in forming tight interactions with bases at the floor of the DNA minor groove. The electrostatic potential molecular surfaces of the structures are similar (Figure 5). The inner face of the molecules with the benzimidazole NH group, which abuts the floor of the minor groove, has significant positive character. The opposite face with the unprotonated benzimidazole N, which faces the solvent, is relatively more negatively charged. This is an advantage for both DB921 and DB911 in both formation of H-bonds and electrostatic interactions with the DNA minor groove.

CONCLUSIONS AND BIOLOGICAL RELEVANCE

We show here that both DB921 and DB911 bind preferably to the minor groove in A·T DNA sequences of ≥4 bp. This is expected for the structure of DB911, which is similar to those of other minor groove binding diamidines (Figure 1). The strong binding of DB921, however, is unexpected on the basis of its lack of appropriate radius of curvature. The dogma from analysis of DNA structure has suggested that compounds outside of a narrow curvature range should not be effective minor groove binding agents. It is, then, particularly surprising to find that DB921 not only binds in the minor groove but has an unusually high binding constant (Table 1).

For therapeutic development, it is essential to design compounds that target A·T sequences in different but effective methods. DB921 represents a new paradigm that does not fit the classical model of minor groove interactions. An induced fit molecular structural change in DB921 reduces the twist of the biphenyl group to complement the minor groove, and places the functional groups in position to interact with DNA bases at the floor of the groove. This, of course, does not correct the lack of curvature of the compound for minor groove binding. This deficiency is solved by incorporating a water molecule into the complex, and the phenyl amidine group contacts the bases at the floor of the groove through indirect contacts involving a bound water. The DB921−water pair forms a curved noncovalent minor groove binding module that matches the shape of the groove.

The thermodynamic analysis of binding of DB921 and DB911 to an AATT DNA sequence shows that the stronger binding of DB921 is due to a more favorable binding enthalpy compared to that of DB911 even though it actually has a slightly less favorable entropy. Previous studies with benzimidazole derivatives have indicated that compounds with even slightly greater curvature than the DNA minor groove could rapidly lose binding energy, and the structural models shown above suggest that this may be the case with DB911. DB921, on the other hand, has an overly small curvature for the minor groove, but the match is improved by induced-fit conformational changes and a bound water molecule that provides a flexible way of linking the phenyl amidine group of DB921 to the floor of the minor groove. This provides a number of additional strong DB921 interactions with DNA that are not possible with DB911. The interactions improve the DB921 enthalpy but decrease the entropy as predicted for incorporation of a bound water (*28*−*30*). This result, along with a previous analysis of a linear diamidine that binds strongly in the minor groove (*16*), clearly suggests that traditional views of the compound curvature required for minor groove complex formation must be reevaluated.

SUPPORTING INFORMATION AVAILABLE

CD spectra, ITC experimental plots, tables of crystallographic data and refinement statistics, and details of the crystallography methods. This material is available free of charge via the Internet at http://pubs.acs.org.

REFERENCES

1. Watkins, B. M. (2003) Drugs for the control of parasitic diseases: Current status and development, *Trends Parasitol. 19*, 477−478.
2. Barrett, M. P., Burchmore, R. J., Stich, A., Lazzari, J. O., Frasch, A. C., Cazzulo, J. J., and Krishna, S. (2003) The trypanosomiases, *Lancet 362*, 1469−1480.
3. Bouteille, B., Oukem, O., Bisser, S., and Dumas, M. (2003) Treatment perspectives for human African trypanosomiasis, *Fundam. Clin. Pharmacol. 17*, 171−181.
4. Tidwell, R. R., and Boykin, W. D. (2003) in *DNA and RNA Binders: From Small Molecules to Drugs* (Demeunynck, M., Bailly, C., and Wilson, W. D., Eds.) Vol. 2, Chapter 16, pp 414−460, Wiley-VCH, New York.
5. Matovu, E., Stewart, M. L., Geiser, F., Brun, R., Maser, P., Wallace, L. J., Burchmore, R. J., Enyaru, J. C., Barrett, M. P., Kaminsky, R., Seebeck, T., and de Koning, H. P. (2003) Mechanisms of arsenical and diamidine uptake and resistance in *Trypanosoma brucei*, *Eukaryotic Cell 2*, 1003−1008.
6. Wilson, W. D., Nguyen, B., Tanious, F. A., Mathis, A., Hall, J. E., Stephens, C. E., and Boykin, D. W. (2005) Dications that target the DNA minor groove: Compound design and preparation, DNA interactions, cellular distribution and biological activity, *Curr. Med. Chem.: Anti-Cancer Agents 5*, 389−408.
7. Klingbeil, M. M., Drew, M. E., Liu, Y., Morris, J. C., Motyka, S. A., Saxowsky, T. T., Wang, Z., and Englund, P. T. (2001) Unlocking the secrets of trypanosome kinetoplast DNA network replication, *Protist 152*, 255−262.
8. Shapiro, T. A., and Englund, P. T. (1995) The structure and replication of kinetoplast DNA, *Annu. Rev. Microbiol. 49*, 117−143.
9. Neidle, S. (2001) DNA minor-groove recognition by small molecules, *Nat. Prod. Rep. 18*, 291−309.
10. Bailly, C., and Chaires, J. B. (1998) Sequence-specific DNA minor groove binders. Design and synthesis of netropsin and distamycin analogues, *Bioconjugate Chem. 9*, 513−538.
11. Fairley, T. A., Tidwell, R. R., Donkor, I., Naiman, N. A., Ohemeng, K. A., Lombardy, R. J., Bentley, J. A., and Cory, M. (1993) Structure, DNA minor groove binding, and base pair specificity of alkyl- and aryl-linked bis(amidinobenzimidazoles) and bis(amidinoindoles), *J. Med. Chem. 36*, 1746−1753.
12. Goodsell, D., and Dickerson, R. E. (1986) Isohelical analysis of DNA groove-binding drugs, *J. Med. Chem. 29*, 727−733.
13. Bailly, C., Tardy, C., Wang, L., Armitage, B., Hopkins, K., Kumar, A., Schuster, G. B., Boykin, D. W., and Wilson, W. D. (2001) Recognition of ATGA sequences by the unfused aromatic dication DB293 forming stacked dimers in the DNA minor groove, *Biochemistry 40*, 9770−9779.
14. Wang, L., Carrasco, C., Kumar, A., Stephens, C. E., Bailly, C., Boykin, D. W., and Wilson, W. D. (2001) Evaluation of the

influence of compound structure on stacked-dimer formation in the DNA minor groove, *Biochemistry 40*, 2511−2521.
15. Nguyen, B., Lee, M. P., Hamelberg, D., Bailly, C., Brun, R., Neidle, S., and Wilson, W. D. (2002) Strong binding in the DNA minor groove by an aromatic diamidine with a shape that does not match the curvature of the groove, *J. Am. Chem. Soc. 124*, 13680−13681.
16. Nguyen, B., Hamelberg, D., Bailly, C., Colson, P., Stanek, J., Brun, R., Neidle, S., and Wilson, W. D. (2004) Characterization of a novel DNA minor-groove complex, *Biophys. J. 86*, 1028−1041.
17. Ismail, M. A., Batista-Parra, A., Miao, Y., Wilson, W. D., Wenzler, T., Brun, R., and Boykin, D. W. (2005) Dicationic near-linear biphenyl benzimidazole derivatives as DNA-targeted antiprotozoal agents, *Bioorg. Med. Chem.* (in press).
18. Ismail, M. A., Brun, R., Wenzler, T., Tanious, F. A., Wilson, W. D., and Boykin, D. W. (2004) Dicationic biphenyl benzimidazole derivatives as antiprotozoal agents, *Bioorg. Med. Chem. 12*, 5405−5413.
19. Myszka, D. G., He, X., Dembo, M., Morton, T. A., and Goldstein, B. (1998) Extending the range of rate constants available from BIACORE: Interpreting mass transport-influenced binding data, *Biophys. J. 75*, 583−594.
20. Karlsson, R. (1999) Affinity analysis of non-steady-state data obtained under mass transport limited conditions using BIAcore technology, *J. Mol. Recognit. 12*, 285−292.
21. Wilson, W. D., Tanious, F. A., Fernandez-Saiz, M., and Rigl, C. T. (1997) Evaluation of drug-nucleic acid interactions by thermal melting curves, *Methods Mol. Biol. 90*, 219−240.
22. Wilson, W. D., Tanious, F. A., Barton, H. J., Wydra, R. L., Jones, R. L., Boykin, D. W., and Strekowski, L. (1990) The interaction of unfused aromatic heterocycles with DNA: Intercalation, groove-binding, bleomycin amplification, *Anticancer Drug Des. 5*, 31−42.
23. Rodger, A., and Norden, B. (1997) *Circular Dichroism and Linear Dichroism*, pp 15−31, Oxford University Press, New York.
24. Davis, T. M., and Wilson, W. D. (2001) Surface plasmon resonance biosensor analysis of RNA-small molecule interactions, *Methods Enzymol. 340*, 22−51.
25. Wilson, W. D. (2002) Analyzing biomolecular interactions, *Science 295*, 2103−2105.
26. Day, Y. S., Baird, C. L., Rich, R. L., and Myszka, D. G. (2002) Direct comparison of binding equilibrium, thermodynamic, and rate constants determined by surface- and solution-based biophysical methods, *Protein Sci. 11*, 1017−1025.
27. Wiseman, T., Williston, S., Brandts, J. F., and Lin, L. N. (1989) Rapid measurement of binding constants and heats of binding using a new titration calorimeter, *Anal. Biochem. 179*, 131−137.
28. Dunitz, J. D. (1994) The entropic cost of bound water in crystals and biomolecules, *Science 264*, 670−670.
29. Copper, A. (2005) Heat capacity effects in protein folding and ligand binding: A re-evaluation of the role of water in biomolecular thermodynamics, *Biophys. Chem. 115*, 89−97.
30. Clarke, C. C., Woods, R. J., Gluska, J., Cooper, A., Nutley, M. A., and Boons, G. J. (2001) Involvement of water in carbohydrate-protein binding, *J. Am. Chem. Soc. 123*, 12238−12247.

BI051791Q